Hindawi
Shock and Vibration
Volume 2021, Article ID 5553914, 14 pages
https://doi.org/10.1155/2021/5553914

Research Article

Energy Action Mechanism of Coal and Gas Outburst Induced by Rockburst

Wenqing Zhang,[1] **Chaomin Mu**,[1] **Dengke Xu**,[2] **and Zhongqing Li**[1]

[1]*School of Safety Science and Engineering, Anhui University of Science and Technology, Huainan 232001, Anhui, China*
[2]*School of Civil Engineering and Architecture, Anhui University of Science and Technology, Huainan 232001, Anhui, China*

Correspondence should be addressed to Chaomin Mu; chmmu@mail.ustc.edu.cn

Received 21 February 2021; Revised 14 April 2021; Accepted 6 June 2021; Published 14 June 2021

Academic Editor: Bangbiao Wu

The essence of both rockburst and coal and gas outburst lies in fast energy release. In order to explore the energy action mechanism of coal and gas outburst induced by rockburst in rockburst and coal and gas outburst combined mines, the split Hopkinson pressure bar (SHPB) experimental device was firstly used to conduct uniaxial impact failure test of coal specimens prone to outburst under different strain rates, and their energy dissipation laws under impact loading were obtained. Next, under the engineering background of coal and gas dynamic phenomena induced by rockburst with different intensities in Xinyi Coal Mine and Pingdingshan Coal Group No. 12 Colliery in Henan Province and Dingji Coal Mine of Huainan Mining Group in Anhui Province, experimental study results were combined with numerical simulation analysis to discuss the energy mechanism of coal and gas outburst induced by rockburst. The study results show that the outburst can be divided into two different processes—critical outburst and outburst—according to the evolution law of outburst energy, and the critical energy conditions for coal and gas outburst are proposed. The minimum destructive energy range for the critical outburst of coal mass is obtained as $(5–10) \times 10^4$ J/m^3. Under some low gas, high stress, or strong disturbance conditions, applied loads can become the main energy sources causing critical failure and even crushing and throwing of coal mass. The coal mass will present an interval splitting structure under dynamic loading, which is obviously different from the failure mode of coal mass under static actions.

1. Introduction

The coal and gas outburst and rockburst are the most serious dynamic disasters in the underground coal mining activities in various countries across the globe [1–6]. In shallow mining, the dynamic disaster is mostly manifested by the single appearance of coal and gas outburst or rockburst, while their interaction is not that prominent, and their prediction and prevention and control are usually separately implemented.

Rockburst usually happens in mining operation and civil engineering. There are diversified rockburst mechanisms, and the main factors are generally related to underground geometrical shape and geological conditions [7–9]. Rockburst in itself is the sudden release of elastic strain energy stored in the rock mass under the excavation unloading effect, and it is an energy-driven dynamic instability phenomenon. Many scholars have investigated the dynamic mechanical behaviors of rockburst based on the energy theory and achieved prominent results. Cook [10] pointed out that energy release was one of the most important factors inducing rockburst and put forward the concept of energy release rate. Mitri et al. [11] proposed the burst potential index, expressing that rockburst would probably happen when the energy storage rate in the rock reached the energy storage limit. As indicated by Wiles [12], local energy release density (LERD) should be combined with the stress conditions to evaluate rockburst; namely, it could be used to predict rockburst only when approaching the stress conditions of rock mass strength. In order to understand rockburst from the angle of energy release, Jiang et al. [13] developed local energy release rate (LERR), which could be

used to predict the rockburst intensity very well. Xu et al. [14] combined LERR and limiting energy storage rate (LESR) to put forward a new energy index—rockburst energy release rate (RBERR).

Coal and gas outburst refers to the outburst phenomenon of mass coal or gas during the coal mining process. In recent hundred years, many scholars have explored this phenomenon, expecting to better understand its formation mechanism. A current viewpoint is that outburst means the intense dynamic instability of coal mass when the interaction of coals with abnormal ground stress, high gas pressure, and "inclination to outburst" reaches the critical conditions. The divergence among different theories lies in the different reasons for reaching the critical conditions of outburst. Many models such as pocket model, dynamic model, and multifactor model have been raised to explain the outburst mechanism [15, 16]. Hodot [17] and Zhao et al. [18] thought that the outburst could be divided into four phases: preparation, trigger, development, and termination. Díaz Aguado and González Nicieza [2] and Guan et al. [19] pointed out that the outburst conditions could be quantified through outburst thresholds such as gas pressure, gas content, and stress. However, it is difficult to estimate the energy participating in the outburst, not to mention to quantify it, because of the complexity of coal and gas outburst.

As the mining depth is increased, the interaction between two disasters—coal and gas outburst and rockburst—has started appearing, and therefore, they tend to coexist and combine each other. Especially in deep high-ground-stress zone, their interaction will be aggravated, which has gradually aroused high attention among domestic (Chinese) and foreign scholars. In rockburst and coal and gas outburst combined mine, the rockburst has induced coal and gas outburst, and the coal and gas outburst induced under low gas pressure has become more and more frequent. The gas concentrations in German Rhein-Westphal Mine, Ruhr Mine, and Husk Mine are elevated abnormally before and after the rockburst [20, 21]. The rockburst and mine earthquake-induced coal and gas outburst or abnormal gas emission have occurred in Laohutai Mine and Beipiao Taiji Mine in Liaoning Province, Hegang Coalfield in Heilongjiang, Huainan Dingji Mine, and Pingdingshan Coal Group No. 12 Colliery, China [22–25].

The former Soviet scholar Petukhov [26] put forward studying the two phenomena—rockburst and outburst—as a whole at the earliest; according to the increasing volume fraction of gas before and after rockburst, Айруни [27] proposed a doubt over whether it was rockburst that induced the increasing volume fraction of gas or it was the increasing volume fraction that induced rockburst or the two coexisted; Ogieglo et al. stated [28] that the gas emission quantity would be elevated when the working face was under vibration. In China, Zhang et al. [29] took the lead in proposing and establishing the theory of unified instability of rockburst and coal and gas outburst and deemed that rockburst was outburst without gas action while outburst was rockburst with nonnegligible gas action. Pan et al. [30] proposed the concept of coal and gas outburst and rockburst combined dynamic disaster, put forward their integrated prediction and control, revealed the unification mechanism for the occurrence of this combined dynamic disaster, and established the judgment criteria for the uniform instability. Li et al. [31], Li et al.[32] and Wang et al. [33] expounded the internal relation, difference, induction and transformation mechanism, and transformation conditions of two disasters—rockburst and outburst at coal seam.

Materials usually show different failure modes and mechanical characteristics under static load and dynamic load conditions [34–36]. The quasistatic characteristics of coal and rock have been widely investigated, but its dynamic failure characteristics have not been fully recognized. Split Hopkinson pressure bar (SHPB) system has been generally used in dynamic tests at high loading rate, in order to determine the dynamic properties of brittle materials like concrete [37], glass [38] and rock [39, 40] under different strain rates. Shan et al. [41] and Liu et al. [42] used the SHPB device to perform impact tests of coal under different strain rates and obtained the failure deformation characteristics of coking coal and anthracite, etc. Mu and Gong [43] and Rong et al. [44] established a dynamic constitutive equation of coal mass and simulated its two damage forms—fast jumping type and slow stepping type—under impact load. Kong et al. [45, 46] studied the dynamic characteristics of gas-containing coal and established the dynamic constitutive equation of the gas-containing coal under impact load.

Both rockburst and coal and gas outburst refer to the fast energy release in essence, so they can be studied together from the aspect of dynamic energy. Under the engineering background of coal and gas dynamic phenomena induced by rockburst with different intensities in Xinyi Coal Mine and Pingdingshan Coal Group No. 12 Colliery in Henan Province and Dingji Coal Mine of Huainan Mining Group in Anhui Province, the SHPB experiment was combined to obtain the coal energy dissipation laws and investigate the energy mechanism for rockburst-induced coal and gas outburst. The judgment criteria for critical energy conditions and critical crushing energy of coal and gas outburst were proposed, thus providing a reference for recognizing and controlling the rockburst-induced coal and gas outburst.

2. Energy Analysis of Coal and Gas Outburst

The final energy condition for the coal seam to experience outburst-type crushing is as below [31]:

$$W_G + W_C + W_\Delta \geq W_P + W_D + W_V + W_B + \Delta K, \quad (1)$$

where W_G is total dilation energy of gas; W_C is elastic energy of coal; W_Δ is energy entering the coal mass from surrounding rocks; W_P is energy consumed to crush coal mass into blocks; W_D is energy absorbed by surrounding rocks nearby the occurrence site of dynamic phenomenon; W_V is energy consumed by the coal vibration in the nearby region (smaller than 10%); W_B is energy consumed by the formation of air blast wave; and ΔK is kinetic energy increased by the blocks.

The outburst process is divided into two different phases—critical outburst and outburst—and the critical energy condition for the coal and gas outburst is presented as follows:

$$W_{G1} + W_C + W_\Delta \geq W_{P1}, \quad (2)$$

where W_{G1} is total dilation energy of free gas; W_C is elastic energy of coal mass; W_{P1} is energy of coal crushing under the critical coal and gas outburst. The conditions for coal and gas outburst can be satisfied and the outburst will occur only when the sum of the energies applied by gas, surrounding rock, or other sudden loads to the coal mass is approximate to or exceeds the energy of coal crushing under critical outburst.

3. Energy Analysis of Coal Crushing under Impact Load

3.1. Impact Test Results. Soft coal extracted from soft layer was crushed; coal powders were sieved via 40-80-mesh screen, placed into a self-made coal compression tank, and finally made into cylindrical coal specimens (draw ratio: about 0.5) on a large rigid press.

This experiment was completed on the Φ75 mm SHPB experimental system, and the device diagram is shown in Figure 1. The diameters of the impact bar, the incident bar, and the output bar are all 75 mm, and the lengths are 0.4 m, 4 m, and 2.5 m, respectively. The bar is made of high strength alloy steel with an elastic modulus of 195 GPa.

The basic parameters and experimental conditions of the specimen are shown in Table 1.

The crushing forms of coal specimens after the impact are shown in Figure 2.

According to the energy theory of stress wave, the size effect of different specimens was eliminated, and the relationship between coal crushing energy density and strain rate was calculated as seen in Figure 3.

It can be seen that the crushing energy density of each coal specimen presented an exponential increase with the strain rate, and their fitting relation could be expressed by.

$$w_d = 0.05e^{0.012\dot{\varepsilon}}. \quad (3)$$

In general, the mass-frequency distribution in crushed coal follows the following law:

$$\frac{M(R)}{M} = 1 - \exp\left[-\left(\frac{R}{R_0}\right)^b\right], \quad (4)$$

$$b = \frac{\lg(M(R)/M)}{\lg R}, \quad (5)$$

where $M(R)$ is accumulative mass of crushed coal with diameter of smaller than R, kg; M is total mass of crushed coal, kg; R_0 is average size, mm. According to literature [47], $D = 3 - b$, and D is fractal dimension of crushed coal, while b is the slope of the line drawn by $M(R)/M - R$.

Standard screen was used to screen the experimental fragments, and the mesh diameters were 0.5, 1, 10, 20, and 30 mm, respectively. According to (4) and (5), the fractal dimension of experimental fragments is calculated, as shown in Table 2.

The relationship between fractal dimension and crushing energy density of crushed coal specimens is seen in Figure 4.

With the increase in the impact load intensity, the degree of crushing was elevated after the coal failure, the proportion occupied by tiny fragments was significantly enlarged, and the fractal dimension presented a logarithm growth relation with the crushing energy density, indicating that the higher the degree of specimen crushing, the higher the intensity of impact load needed. This is basically identical with the conclusions drawn in other literatures with respect to fractal characteristics of rock and anthracite, etc. under impact failure.

The average particle size of crushed specimens can be expressed by.

$$\overline{d} = \frac{\sum \overline{d}_i \eta_i}{\sum \eta_i}, \quad (6)$$

where $\overline{d}_i$ is average size of crushed blocks retained in a sieve with some specifications during the sieving process, mm; η_i is mass percentage of crushed blocks intercepted in the sieve with the corresponding pore diameter, %.

As the sudden load energy was increased, the average size of crushed blocks was rapidly reduced, and there was a turning point. It could be seen from Figure 5 that when the experimental strain rate exceeded 200 s and the crushing energy density of sudden load reached 6.5×10^5 J/m^3, the average particle size of crushed blocks was approximately unchanged; at the time, the specimen was completely crushed into powders with extremely uniform distribution, and the energy required by the further crushing presented an exponential growth. This coincides with appearance and separation of coal powders following the coal and gas outburst in soft coal.

3.2. Critical Crushing Energy. According to the study of Hu [48] regarding the crushing energy of coal mass, the following can be obtained:

$$W_P = 46914\rho f^{1.437} Y^{1.679}, \quad (7)$$

where f is firmness coefficient of coal mass; Y is mass percentage occupied by coal specimens with particle size of below 0.2 mm after crushing in the total mass of coal specimens. In consideration that the coal mass will be further crushed after the outburst, the Y value under critical outburst should be much smaller than that after the outburst. The relationship between crushing energy of Tolsti coal seam and particle size of coal specimen is listed in literature [49]. When the crushing energy is 7×10^4 J/m^3, the mass percentage occupied by coal specimens with particle size of below 0.375 mm in the total mass of coal specimens is 1.28%, 1.57% under crushing energy of 12×10^4 J/m^3, and 2.2% under crushing energy of 16×10^4 J/m^3. Therefore, Y value is taken as 2.0 under critical outburst, and W_P is 5.6×10^4 J/m^3 when the firmness coefficient f is 0.4.

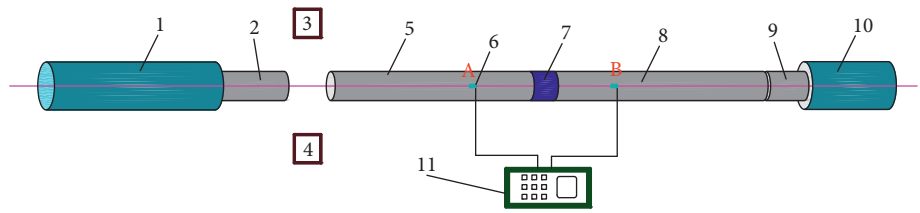

Figure 1: Sketch map of split Hopkinson pressure bar testing system. 1: air cannon; 2: drop bar; 3: laser unit; 4: laser receiver; 5: incident bar; 6: resistance strain gage; 7: test specimen; 8: transmission bar; 9: absorbing bar; 10: bumper; 11: superdynamic strain gauge.

Table 1: The basic parameters and experimental conditions of the specimen.

Serial number	Quality (g)	Height (cm)	Diameter (cm)	Draw ratio	Bullet velocity ($m \cdot s^{-1}$)	Strain rate (s^{-1})
1	85.5	3.61	5	0.72	1.877	73
2	80.4	3.39	5	0.68	4.108	78
3	79.9	3.37	5	0.67	4.032	81
4	79.2	3.36	5	0.67	6.203	101
5	79.6	3.38	5	0.68	6.416	115
6	79.8	3.4	5	0.68	7.175	129
7	79.4	3.34	5	0.67	8.903	160
8	78.9	3.36	5	0.67	7.417	174
9	79.3	3.36	5	0.67	10.36	193
10	77.5	3.24	5	0.65	8.523	214
11	69	2.84	5	0.57	8.602	219
12	80.9	3.49	5	0.70	10.81	221
13	72.7	3.03	5	0.61	9.723	268
14	74.6	3.07	5	0.61	9.79	279

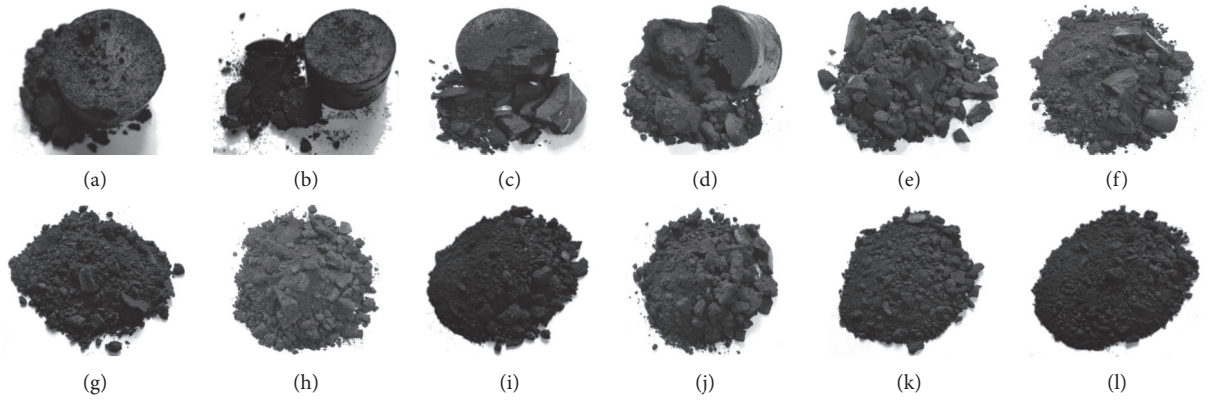

Figure 2: Specimens after impact. (a) 78 s. (b) 81 s. (c) 102 s. (d) 115 s. (e) 129 s. (f) 160 s. (g) 174 s. (h) 193 s. (i) 214 s. (j) 219 s. (k) 268 s. (l) 279 s.

As shown in Figure 1, the experimental strain rate corresponding to the critical state (crushed but not dispersed) of coal mass was about 80/s, and its actual crushing energy was about 9×10^4 J/m^3. Based on the fractal results of impact lumpiness, $Y \approx 2$, $f = 0.6$, and $\rho = 1.4$ kg/m^3, which were substituted into (6) to obtain the critical crushing energy of coal mass as 1.01×10^5 J/m^3, which was very approximate to the experimentally measured crushing energy. Therefore, the critical crushing energy of coal with $f = 0.6$ was about 1×10^5 J/m^3. However, the coal masses from different sources with different coal qualities have different hardness values and f values, so their critical crushing energies will also be different. Hence, no unified judgment criteria for critical crushing energy have been proposed. Nevertheless, outburst coals are generally soft, their f values will not be that different, so a standard scope of critical crushing energy can be given as about (5–10) $\times$ 10^4 J/m^3.

4. Numerical Simulation and Field Analysis of Rockburst-Induced Coal and Gas Outburst

4.1. Modeling. LS-DYNA software was used in this numerical simulation. LS-DYNA software is a general explicit

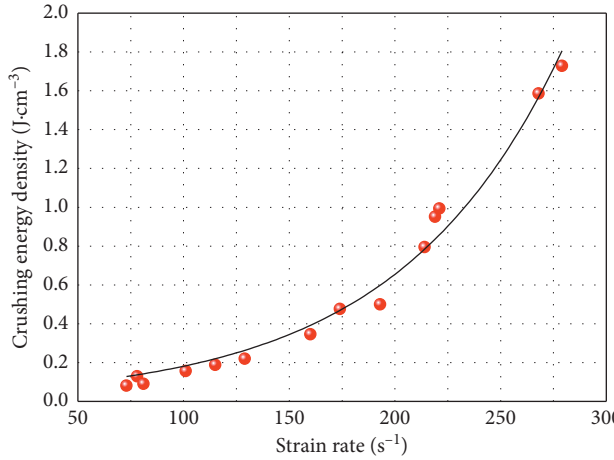

Figure 3: Relationship between crushing energy density and strain rate.

Table 2: Fractal dimension of fragment after impacting outburst coal.

Serial number	Strain rate (s^{-1})	b	Fractal dimension D	Correlation coefficient R
1	73	0.63	2.37	0.990
2	78	0.59	2.41	0.962
3	81	0.58	2.42	0.992
4	102	0.49	2.51	0.999
5	115	0.44	2.56	0.996
6	129	0.45	2.55	0.995
7	160	0.43	2.57	0.991
8	174	0.40	2.60	0.986
9	193	0.44	2.56	0.996
10	214	0.36	2.64	0.959
11	219	0.37	2.63	0.983
12	221	0.38	2.62	0.992
13	268	0.36	2.64	0.955
14	279	0.36	2.64	0.966

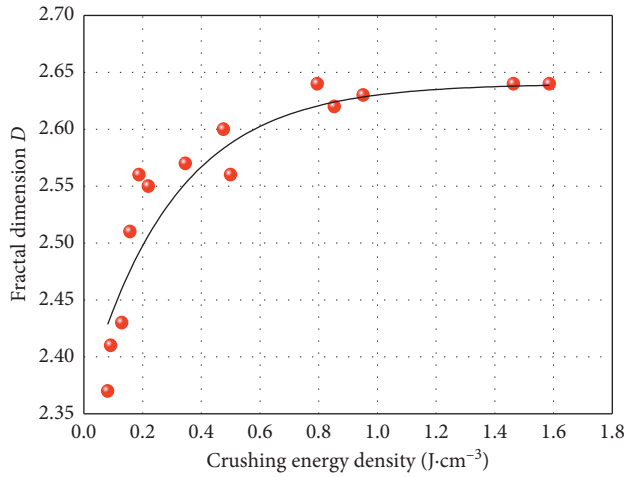

Figure 4: Relationship between fractal dimension and crushing energy density.

dynamic analysis program, especially suitable for solving a variety of two-dimensional and three-dimensional nonlinear structure of high-speed collision, explosion, and other nonlinear dynamic impact problems.

The driving working face was taken as the study object to investigate the failure characteristics of coal mass under the action of external sudden load. The model specification was 15 m × 10 m, where the thickness of both roof and floor was 3 m, the thickness of coal seam was 4 m, and the concrete geometric dimensions are shown in Figure 6.

The basic physical and mechanical parameters of the model are listed in Table 3.

According to related studies [50], the stress wave caused by impact load can be simplified into a triangular pulse load through the propagation for a certain time as shown in Figure 7.

The dynamic constitutive equation of coal mass constructed in literature [42] was embedded into the large-scale finite element analysis software to numerically simulate the coal damage under sudden loading action with peak intensities of $P_{max} = 30$ MPa, 50 MPa, and 70 MPa. Meanwhile, the cases of coal and gas outburst occurring in domestic coal mines in recent years are sorted out, and the three most similar cases are selected (shown in Figure 8). By comparing the results of SHPB experiment and numerical simulation, the coal body fracture characteristics and energy dissipation laws in the process of coal and gas

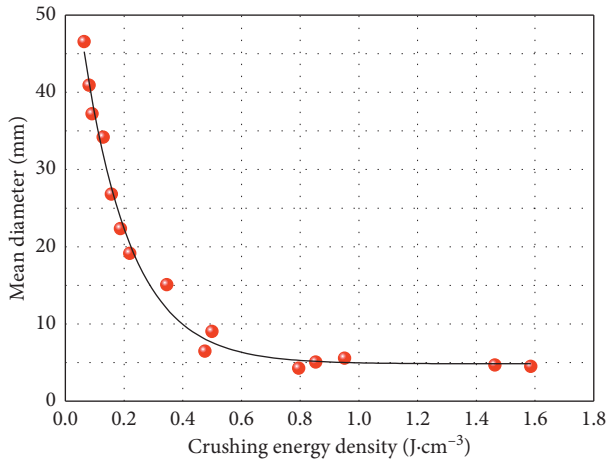

Figure 5: Relationship between mean diameter and crushing energy density.

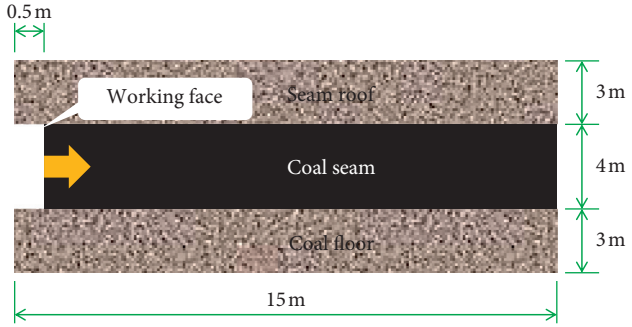

Figure 6: Dimensions of numerical model.

Table 3: Basic parameters of the model.

Parameter	Value
Elastic modulus of rock (GPa)	40
Poisson ratio of rock	0.25
Density of rock (kg·m^{-3})	2300
Cohesion of rock (MPa)	20
Internal frictional angle of rock (°)	27
Elastic modulus of coal (GPa)	20
Poisson ratio of coal	0.4
Density of coal (kg·m^{-3})	1400
Cohesion of coal (MPa)	2.5
Internal frictional angle of coal (°)	40

outburst caused by impact loads of different intensities were explored.

4.2. Numerical Simulation and Case Analysis under Suddenly Applied Load of 30 MPa

4.2.1. Numerical Simulation. When the impact load of 30 MPa was applied to the coal mass at rate of 4 ms, it could be seen from the numerical simulation results that the first oblique crack appeared on the coal mass until 3.908 ms as shown in Figure 9(a), because of loading delay caused by the

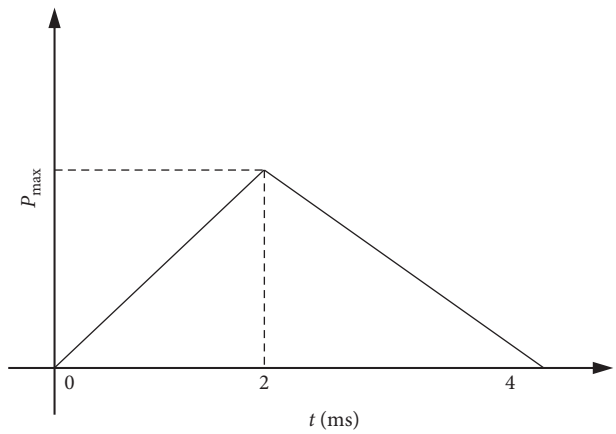

Figure 7: Load time-history curves.

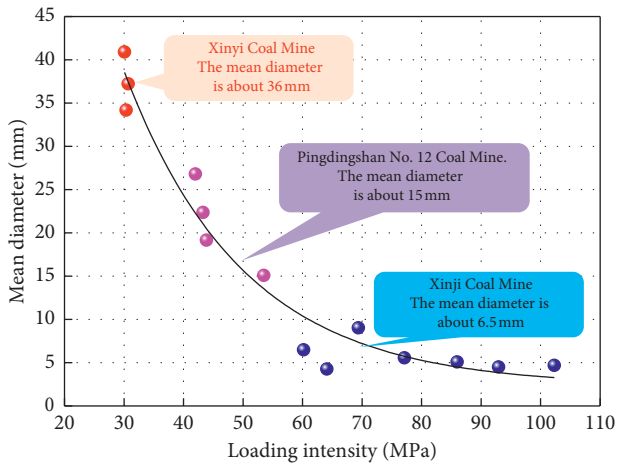

Figure 8: Relationship between mean diameter and loading intensity.

propagation of stress wave in the coal mass for a certain time. With the continuous loading of stress wave until 4.887 ms, the second oblique crack appeared and ran through the first crack, thus providing a channel for gas migration and desorption, and at the time, the coal permeability started increasing as shown in Figure 9(b). With the propagation of stress wave in coal mass, the compression wave would be transformed into tensile stress wave when encountering reflectors like cracks, thus causing further tensile failure of coal mass; new cracks were continuously formed until the energy of stress wave was exhausted at 14.66 ms; multilayered annular cracks were formed in the coal mass nearby the loading end, which damaged the remote coal mass to a certain extent; and microcracks were then formed as shown in Figure 9(f).

From the SHPB experiment, the experimental strain rate was about 80/s when the external load intensity was 30 MPa in the simulation, and the crushing energy input into the coal mass was about 9×10^4 J/m^{-3}. According to the impact test results, the load intensity was not enough to cause the specimen failure, and only some crushed blocks were peeled off as shown in Figure 10. The coal mass could still keep intact, broken, but not dispersed, which was

Figure 9: Numerical simulation under rockburst of 30 MPa. (a) 3.908 ms; (b) 4.887 ms; (c) 5.865 ms; (d) 6.844 ms; (e) 7.822 ms; (f) 14.66 ms.

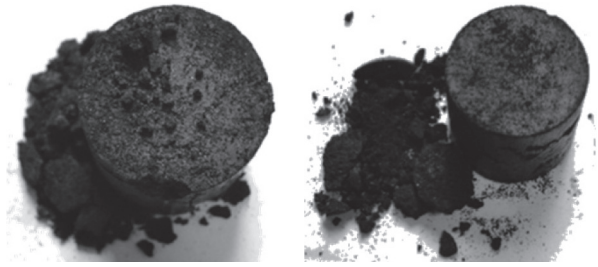

Figure 10: SHPB experimental results at strain rate of about 80 s. (a) 78 s. (b) 81 s.

embodied by dynamic phenomena like sound and slagging from a macroscopic perspective. Meanwhile, cracks were increased in the coal mass with enhanced gas permeability, but restricted by the gas desorption rate, and the emission amount presented a certain time delay and persistence.

4.2.2. Outburst Case Analysis: Outburst Accident on Driving Working Face 12011 Belt Roadway in Xinyi Mine, Henan Province. On July 11, 2009, when the blasting driving construction was implemented at about 21 m of 12011 belt roadway from the crossheading port in Xinyi Mine, Henan Province, coal blasting with loud sound took place continuously at 111 m of working face of this belt roadway from the crossheading port after the blasting continued for 130 min. After another 10 min, the abnormal gas emission exceeded the limit, the maximum concentrate reached about 11%, and the total gas emission was about 700 m^3, without significant coal falling or coal outburst. At 1 h, the gas concentration declined to below 1%.

It was found through the field reconnaissance that the head-on coal mass on the working face was shifted outside for about 50 cm, and a crack with length of about 8 m, width of about 6 cm, and detectable depth of about 1 m appeared on the floor 16 m away from the head-on place as shown in Figures 11 and 12.

The geodetic survey data of the coal mine showed that the gas content at this coal seam was 8.38–12.84 m^3/t (average content: 9.86 m^3/t), the gas pressure was 0.57–1.25 MPa (average pressure: 0.81 MPa), and the coal was soft with firmness coefficient of $f = 0.22$–0.65 (average value: 0.35). Before the coal blasting occurred, the gas concentrations in both head-on place and return air of the belt roadway were lower than 0.5%. In addition, no large rupture and fold structures existed in the scope of the mine, and no apparent geological structures were seen nearby the occurrence site of dynamic phenomenon. It could be

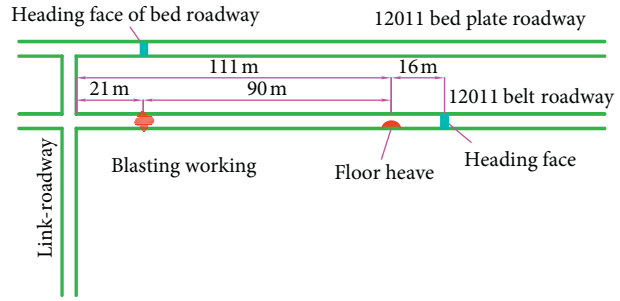

Figure 11: Location of coal and gas dynamic phenomenon in Xinyi Mine, Henan Province.

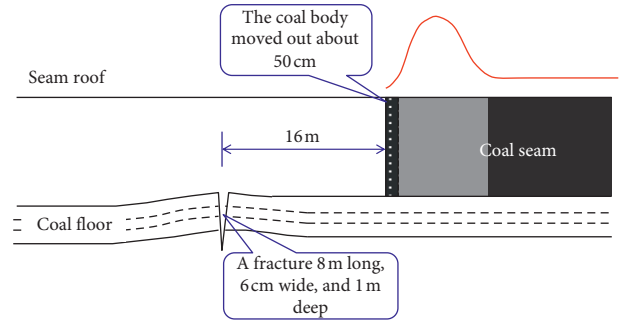

Figure 12: Profile map of working face outburst.

inferred that the gas dynamic phenomenon was triggered by floor fracture-type rockburst.

According to the field microearthquake observation results, the energy generated by the rockburst triggered by this floor fracture was about 1×10^5 J. The existing studies have shown that the energy used to generate vibration and received by the monitoring equipment in the formation of primary rockburst accounts for about 5%–10% in the total energy. If calculated by 10%, here the energy generated by this rockburst was about 1×10^6 J. In addition, the

occurrence source of floor fracture was only 16 m from the location of gas dynamic phenomenon, and it could be approximately deemed that the impact energy generated by the vibration was totally input into the nearby coal mass without attenuation.

Furthermore, the outward shift of head-on coal mass triggered by rockburst was about 0.5 m, while the sectional area of working face was 18.9 m^2, and then the total volume of coal mass experiencing outward shift was about 9.5 m^3. Hence, the energy density input by rockburst into the coal mass could be estimated as 1.05×10^5 J/m^{-3}. By combining the field gas data, the gas content and gas pressure in the coal seam were $Q = 9.86$ m^3/t and $P_0 = 0.74$ MPa, respectively. According to literature [47], the dilation energy of gas participating in the coal failure could be calculated as 2.3×10^4 J/m^3.

To sum up, in this dynamic phenomenon, the total energy of gas and external rockburst acting upon the coal mass was about 1.28×10^5 J/m^{-3}, which was slightly greater than the minimum energy intensity criterion needed by the critical failure of coal mass as given in the previous part. Therefore, it was just enough to trigger the failure, but the coal mass was crushed but not dispersed, and internal cracks were generated, which provided a channel for the gas migration and desorption. By a comparison between the two input energies, the dilation energy of gas was only 1/5 of the impact vibration energy, so the main energy source triggering this dynamic phenomenon was rockburst caused by the floor fracture. Meanwhile, as the gas pressure was low at the coal seam, the generated minimum dilation energy of gas was not enough to trigger the coal outburst, no coal mass was thrown out, but only abnormal gas emission took place.

As the desorption of adsorbed gas is a slow process while the free gas only accounts for about 10% of total gas, the gas emission on the site showed a certain time delay and continuity, the gas concentration exceeded the limit after 10 min, reaching about 11%, and after about 1-2 h, about over 90% of the gas inside the coal mass was desorbed and released, and the field gas concentration was gradually recovered to below 1%.

4.3. Numerical Simulation and Case Analysis under Suddenly Applied Load of 50 MPa

4.3.1. Numerical Simulation. When the simulated load intensity reached 50 MPa, the crack propagation was obviously aggravated in the coal mass. Multilayer annular spalling occurred in the coal mass at near loading end at 5.862 ms as shown in Figure 13(c). The coal mass started crushing since 6.841 ms, and the crushing was continuously aggravated and extended till the roof of coal seam as shown in Figure 13(f). Apparent cracks appeared at the far end of coal mass.

From the SHPB experiment, the experimental strain rate was about 160/s when the intensity of external applied load reached 50 MPa, and the crushing energy input into the coal mass reached about 3.5×10^5 J/m^{-3}. The energy input into the coal mass was enough to trigger the coal failure and instability, and the coal was crushed into large blocks as shown in Figure 14. After the coal mass was crushed, the crushed coal mass was damaged and peeled off the coal wall and even thrown out for a certain distance under the releasable elastic latent energy accumulated in the coal mass and internal energy of gas.

4.3.2. Outburst Case Analysis: Outburst Accident during the Driving Process on the Working Face of 17310 Conveyor Lane in Pingdingshan Coal Group No. 12 Colliery. At 17:00 on March 19, 2006, the coal and gas dynamic phenomenon triggered by the rockburst occurred after the blasting operation on the working face of 17310 conveyor lane in Pingdingshan Coal Group No. 12 Colliery as shown in Figure 15.

Through the field reconnaissance, the coal and gas dynamic phenomenon presented the following characteristics: (1) about 46 t of coal mass was thrown out, without separation phenomenon; the throwing angle of coal mass was close to the natural angle of repose, the stacking length along the roadway was 5.6 m, where the first 4.0 m showed complete-roadway stacking, and the remaining 1.6 m presented half-roadway stacking. (2) Above the stacked coal and rock was a layer of crushed coal blocks, and there was a small quantity of crushed coal inside the coal and rock, without separability. (3) From the thrown crock and rock and stacking status, there was no gas channel. (4) No floating dust was stacked on the surface or at rear part of the thrown surface. (5) The total gas emission was 1,280 m^3, which was converted into gas emission per ton of coal of 28 m^3/t, approaching the gas content at the coal seam. (6) The coal wall at left of the roadway bulged for 0.9 m; obvious deformation of trapezoid beam and reinforcing mesh triggered by outward impact force could be observed at the roadway roof, the tapered end of anchor rope was loosened, and obvious nonuniform subsidence took place at the immediate roof. The upper-wall trapezoid beam was deformed; the scraper conveyor on the floor deviated towards the right wall of roadway for 5°, and the maximum displacement reached 0.9 m. The overall outward shift of coal wall was observed at the lower wall of the head-on roadway and outward head-on roadway, the displacement and thickness of the lower wall were 10 m and 0.8 m, respectively, the floor bulged for 0.5 m, and the head-on place was shifted out of the wall mass for 3 m. Therefore, the power source for this dynamic phenomenon mainly came from the left side of the roadway.

The elevation of the working face in 17310 conveyor lane where the coal and gas dynamic phenomenon happened was −1,100 m, and it was located at the lower segment of Likou large syncline under serious influence of tectonic stress. The immediate roof of this coal seam consisted of sandstone and mudstone with an average thickness of 0.8 m, while the upper roof was composed of sandstone and fine sandstone with average thickness of 8.0 m. The coal seam was dry and brittle, the coal failure types were II-III, and the firmness coefficient of coal was $f = 0.4$–1.5. Influenced by the mining-induced stress like roadway blasting excavation and

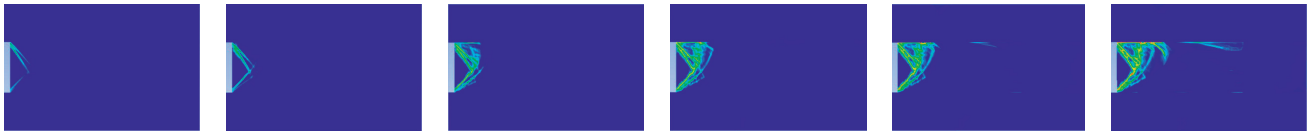

Figure 13: Numerical simulation of rockburst under load of 50 MPa. (a) 3.907 ms; (b) 4.884 ms; (c) 5.862 ms; (d) 6.841 ms; (e) 7.819 ms; (f) 14.66 ms.

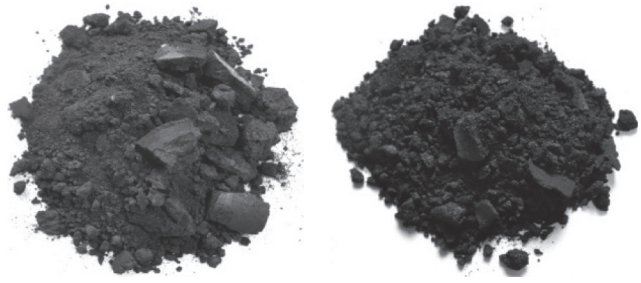

Figure 14: SHPB experimental results under strain rate of about 160 s. (a) 160 s. (b) 174 s.

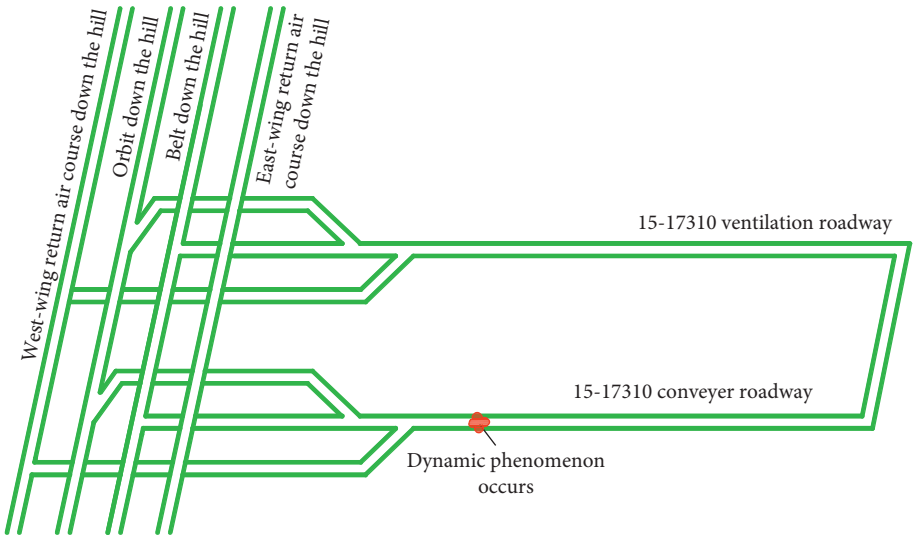

Figure 15: Location of dynamic phenomenon in 17310 conveyor lane of Pingdingshan Coal Group No. 12 Colliery.

tectonic stress, stress concentration could be easily formed in the coal mass behind the working face, and thus a large quantity of elastic latent energy was accumulated. When the coal and rock mass reached or exceeded the ultimate strength, the coal mass would experience a failure. The gas occurring in the coal mass released gas energy with the fracture of coal mass, and the energy superposition at the time created conditions for the coal and gas dynamic phenomenon.

Given this, this was a gas dynamic phenomenon induced by the rockburst in the zone with high ground stress, concentrated stress, and gas pressure.

From the gas data, the gas pressure in the coal seam was 0.74 MPa (after the antioutburst measures were taken), and the dilation energy of gas participating in the coal failure could be calculated as about 4.68×10^4 J/m^3, which was approximate to the lower limit of the standard scope ($(5\sim10) \times 10^4$ J/m^3) of critical crushing energy as given in the previous part, indicating that this outburst is the product of joint action of gas and external applied load. Moreover, due to high gas content in the coal seam, a large quantity of gas was released after the critical failure, the coal mass was further crushed and thrown out, and thus a large quantity of coal mass was extruded out.

4.4. Numerical Simulation and Case Analysis of Rockburst under Suddenly Applied Load of 70 MPa

4.4.1. Numerical Simulation. From the numerical simulation results, the coal crushing speed was significantly

accelerated when the intensity of applied load reached 70 MPa in comparison with the previous two circumstances. The coal mass at loading end presented multiple layered cracks at 3.906 ms, the cracks basically ran through each other at 5.863 ms, and multilayer annular spalling was generated as shown in Figures 16(a)–16(c) With the continuous and reciprocal propagation of stress wave, the original cracks were further stretched, and meanwhile, the surrounding coal mass experienced continuous tensile failure, and the cracks were extended to deep parts. Since 6.842 ms, as a large quantity of elastic latent energy was stored in the coal mass within the stress concentration zone in front of the working face, the coal mass was crushed when the energy storage limit (namely, ultimate strength) of the coal mass was exceeded. Moreover, the elastic latent energy was continuously released outward, thus damaging the surrounding coal mass as shown in Figures 16(d) and 16(e). The surplus elastic latent energy and released internal energy of gas further acted upon the crushed coal mass, so the crushed coal mass in the pressure relief zone was continuously peeled off the coal wall and even thrown towards the exterior space. Moreover, a wedge-shaped hole with large mouth and small cavity might be formed on the coal mass. In the later loading phase as shown in Figure 16(f), the coal failure was aggravated with the continuous energy release, the supporting stress was reduced and the roof and floor nearby the coal mass started experiencing failures, along with dynamic phenomena like roof caving or floor bulging deformation. As the releasable elastic latent energy stored in the coal mass was gradually released and exhausted, the coal and rock continuously stacked in the hole formed greater and greater supporting force on the hole wall, so the coal mass around the hole wall was not further fractured, and the outburst process became unsustainable and was even terminated.

From the SHPB experimental results, the strain rate was about 200/s and the crushing energy input into the coal mass reached about 6.5×10^5 J/m^{-3} when the intensity of external applied load reached 70 MPa. At the time, the energy input could trigger the intense coal failure, and the coal might be even crushed into powders as shown in Figure 17.

4.4.2. Outburst Case Analysis: Outburst Accident on the Working Face of 1331 (1) Conveyor Lane in Dingji Mine. The working face of 1331 (1) conveyor lane where the accident occurred was located in east No. 2 mining area of Dingji Mine, and the burial depth and coal thickness were 870 m and 2.1-2.2 m, respectively. At the roof was sandy mudstone with a thickness of 6.0 m, and at the immediate floor was mudstone with thickness of 3.6 m. The excavation team was on the scene of this accident, and the pattern of two rows per cycle was adopted. The one-cycle construction and anchor bolt supporting were already completed at about 18: 40, and the second-cycle drivage was started. At 19:40, the coal mass was thrown out in right front of the working face. The roof wall zone at right of the roadway presented irregular hemiellipsoidal collapse, the top steel belts in the first row at the left wall of the driving working face were exposed forward on the roof for 1.6 m (there were cutting nicks of roadheader at the roof of the working face), the right wall caved forward for 4.6 m, and the maximum caving height was 1.7 m. An irregular hole appeared above the coal mass at the interface between right wall and working face on the field, with diameter of 0.65 m and depth of about 3 m, and the horizontal distance from the center line of hole to the extension cord of the right wall of the roadway was 1.5 m as shown in Figure 18. The gas concentration in the hole was about 0.8%.

The disaster triggered by gas dynamic phenomenon showed the following characteristics.

The maximum value of gas concentration sensor T2 on the working face was 2.02% after the dynamic phenomenon. Through the calculation, the total gas emission and coal quantity were 235.4 m^3 and 35 t, respectively; due to this dynamic phenomenon, the average gas emission per ton of coal was 6.7 m^3/t, which was smaller than the standard; namely, the gas emission per ton of coal in the coal and gas outburst was greater than 30 m^3/t or twice the gas content in the coal seam. Moreover, except for the deaths caused by coal burying, other deaths on the accident scene had no sign of asphyxia, and the gas concentration at the bottom of cavity formed by the dynamic phenomenon was about 0.8% after the accident took place for 135 h.

Before the accident took place, there was no coal blasting sound during the working shift, and the gas concentration in the return air did not experience any abnormal change. The right wall of the roadway and the coal wall on the working face were caving, where the right wall caving width of the roadway was about 1.6 m, and the maximum depth was 0.5-0.6 m. The coal wall caving width and depth in right front of the working face were about 2 m and 0.9 m, respectively.

The driver of roadheader heard a sound of "bang," just like blasting sound when the accident occurred. The field staffs felt vibration and blast, the air duct was obviously agitated, the well-connected metal net was not torn open, and the air duct and existing supporting facilities were not obviously damaged.

Partial coal mass was thrown out, and the distance from stacked coal to the working face was 4–6 m. The cavity formed after the coal mass was thrown out was located the interfacial zone (wedge shape) between right wall and coal wall of the working face, with width of about 3-4 m and depth of 6-7 m, and it presented pinching-out towards the deep part. After the coal and gangues were cleared away from the field, the residual cavity was about 0.65 m in width and 3 m in depth, and there was a split fissure surface at the coal seam inside the cavity with clear stratification as shown in Figure 19. The coal stacked on the field had no obvious separation phenomenon, which was obviously different from the traditional coal fracture form induced by coal and gas outburst.

By comparing Figures 16 and 19, it could be found that the coal mass generated vertical split cracks under the impact load, and the cracks were under interbed interval distribution. With the increase in the impact load, the through cracks (red region in the figure) were wedge-shaped, seriously damaged wedge-shaped through cracks were

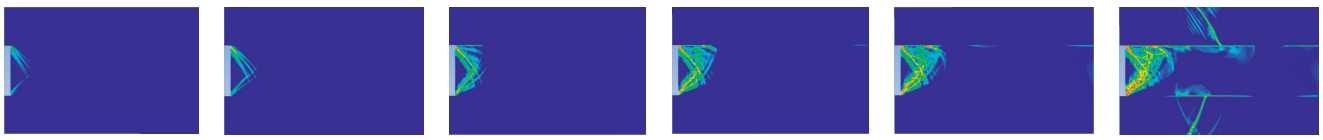

Figure 16: Numerical simulation of rockburst under load of 70 MPa. (a) 3.906 ms; (b) 4.884 ms; (c) 5.863 ms; (d) 6.842 ms; (e) 7.82 ms; (f) 15 ms.

Figure 17: SHPB experimental results under strain rate of about 210 s. (a) 214 s. (b) 219 s.

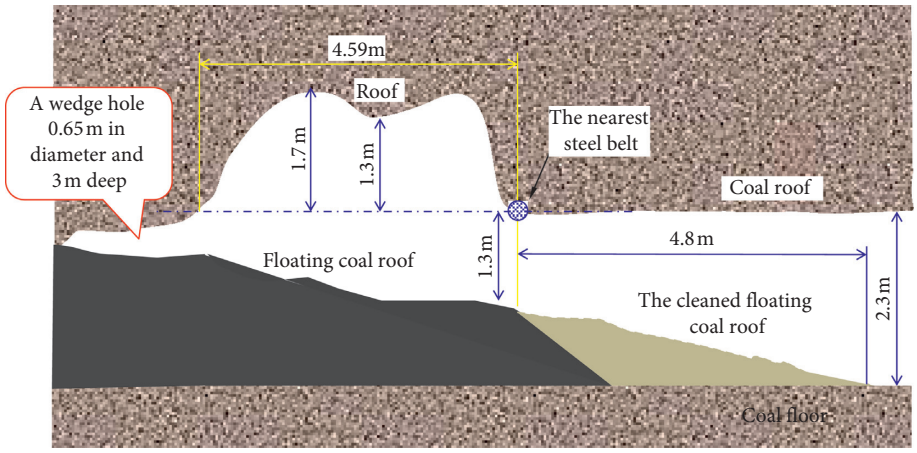

Figure 18: Profile map of outburst accident scene.

generated at 2-3 m from the free face of the coal mass, and these cracks were basically identical with the shape and location of wedge-shaped holes found on the field. The coal and rock crushing under the impact load generated larger particle size than the traditional gas-dominated outburst coal and rock crushing did, and the outburst holes were not traditional "pyriform" holes with small mouth and large belly, but instead, they were wedge-shaped.

There was a normal fault with drop height of 0.9 m at 16.7 m away behind the working face, and the working face was located at its footwall but still in the tectonically affected zone. As predicted by the geodetic survey department, the coal seam was thinned at 3-4 m in front of the working face where the accident took place, and minor structures were quite developed.

To sum up, this was a dynamic disaster of coal outburst caused by local rockburst during the excavation process of the working face under large burial depth and high ground stress of coal seam in the tectonically affected zone. According to the field gas data, the gas content and gas pressure in the coal seam were $Q = 5.2\,\mathrm{m^3/t}$ and $P_0 = 0.74$ MPa, respectively, and the dilation energy of gas participating in the coal failure was only $1.13 \times 10^4\,\mathrm{J/m^3}$, which was different from the previously given critical coal crushing energy of $(5–10) \times 10^4\,\mathrm{J/m^3}$ by orders of magnitude. Hence, the main energy leading to the critical coal failure in the coal and gas outburst was not dilation energy of gas but the energy applied by the intense external load on the coal mass. By combining the above numerical simulation, it could be known that when the impact load was large (like 70 MPa), the coal mass would not only present stratiform splitting until being extruded out. Moreover, the surplus elastic latent energy could also cause the roof and floor failure, so the dynamic phenomena like roof caving or floor

(a) (b)

Figure 19: Coal fracture form under impact load. (a) Roadway; (b) coal body.

bulging deformation would take place, which was very identical with this case.

Based on the above numerical simulation of coal damage under the loading action with intensities of 30 MPa, 50 MPa, and 70 MPa and combining the corresponding field cases and energy calculation, it can be found that the coal and gas outburst is caused by the coaction of dilation energy of gas and external applied load (like excavation, blasting, tectonic stress, surrounding rock stress, etc.). Under low gas content, high stress, or strong disturbance, the external applied load can become the main energy source for the critical coal failure, and even crushing and throwing. Meanwhile, it is verified through the field measured data that the proposed standard scope ($(5–10) \times 10^4$ J/m^3) of the minimum coal crushing energy needed by the critical outburst is reasonable.

It can be seen that, in different geological conditions and mining conditions, the risk of coal mine disaster is very different. The influence of geological conditions on rockburst and gas outburst is mainly shown in the following. (1) Normal fault is formed by tensile stress, there is no energy accumulation in the layer, and it has little influence on rockburst and gas outburst. The mechanism of rockburst and gas outburst induced by normal faults is mainly stress superposition. (2) Since the reverse fault is formed by compression, the rock layer accumulates a lot of elastic energy in the process of compression. Therefore, the release of elastic energy is easy to induce rockburst and gas outburst. (3) Because the fold is formed by horizontal stress extrusion, there will be residual stress and elastic energy in the rock mass in the fold area. The further release of elastic energy is an important factor causing rockburst and gas outburst. (4) When the hardness, thickness, and dip angle of the coal seam changed, the stress concentration of the surrounding rock mass is easy to appear. When the mining face is close to these areas, it is prone to cause stress superposition, which may lead to the occurrence of rockburst and gas outburst.

In order to ensure mining safety, commonly used goaf gas extraction methods include (1) buried tube extraction; (2) high drilling extraction; (3) high lane extraction; (4) surface borehole extraction.

When the sealing of the roof and floor is good, and in the stress concentration area, it is more likely to lead to the occurrence of rockburst and gas outburst. With the increase of mining depth, the coupled disaster of stress and gas will increase, which is the focus of the next research.

5. Conclusions

(1) Through the energy analysis of outburst process, the outburst process can be divided into two different processes: critical outburst and outburst, and the critical energy condition for the coal and gas outburst is proposed as $W_{G1} + W_C + W_\Delta \geq W_{P1}$. In other words, the initiating conditions for the coal and gas outburst can be met and the outburst can occur only when the sum of energies applied by gas, surrounding rock, or other suddenly applied loads to the coal mass is approximate to or exceeds the coal crushing energy in the critical outburst. By combining the experimental results of coal mass under the impact load and predecessors' study results, the scope of minimum coal crushing energy for the critical outburst is proposed, namely, $(5–10) \times 10^4$ J/m^3.

(2) Based on a comparative analysis of numerical simulation and field cases, the coal and gas outburst is caused jointly by the dilation energy of gas and external applied load (such as excavation, blasting, tectonic stress, and surrounding rock stress). Under low gas content, high stress, or strong disturbance, the external applied loads can become the main energy source for the critical coal failure and even crushing and throwing.

(3) The evolution process of split cracks under different impact loads is effectively investigated through the numerical analysis of coal impact failure caused by the stress waves with different peak intensities. The study results show that an interval split structure appears in the coal mass under the dynamic loading action, which is evidently different from the failure form of coal mass under static action. With the increase in the peak intensity of stress wave, all the interval splitting damage in different zones presents an enhancement trend, but the enhancement amplitude is varied.

Data Availability

All data included in this study are available upon request by contacting the corresponding author.

Conflicts of Interest

The authors declare that there are no conflicts of interest regarding the publication of this paper.

Acknowledgments

This work was supported by the University Natural Science Foundation of Anhui Province (KJ2017A091, KJ2019A0098, and 1808085ME160).

References

[1] D. J. Black, "Review of coal and gas outburst in Australian underground coal mines," *International Journal of Mining Science and Technology*, vol. 29, no. 6, pp. 815–824, 2019.

[2] M. B. Díaz Aguado and C. González Nicieza, "Control and prevention of gas outbursts in coal mines, Riosa-Olloniego coalfield, Spain," *International Journal of Coal Geology*, vol. 69, no. 4, pp. 253–266, 2007.

[3] L. Yuan, "Control of coal and gas outbursts in Huainan mines in China: a review," *Journal of Rock Mechanics and Geotechnical Engineering*, vol. 8, no. 4, pp. 559–567, 2016.

[4] A. Keneti and B. A. Sainsbury, "Review of published rockburst events and their contributing factors," *Engineering Geology*, vol. 246, pp. 361–373, 2018.

[5] P. Konicek, M. R. Saharan, and H. Mitri, "Destress blasting in coal mining–state-of-the-art review," *Procedia Engineering*, vol. 26, pp. 179–194, 2011.

[6] J. Ptáček, "Rockburst in Ostrava-Karvina coalfield," *Procedia Engineering*, vol. 191, pp. 1144–1151, 2017.

[7] W. D. Ortlepp and T. R. Stacey, "Rockburst mechanisms in tunnels and shafts," *Tunnelling and Underground Space Technology*, vol. 9, no. 1, pp. 59–65, 1994.

[8] W. L. Zhang, N. J. Ma, and J. Ma, "Mechanism of rock burst revealed by numerical simulation and energy calculation," *Shock and Vibration*, vol. 2020, Article ID 8862849, 15 pages, 2020.

[9] M. T. Gao, Z. Q. Song, and H. Q. Duan, "Mechanical properties and control rockburst mechanism of coal and rock mass with bursting liability in deep mining," *Shock and Vibration*, vol. 2020, Article ID 8833863, 15 pages, 2020.

[10] N. G. W. Cook, "The design of underground excavations," in *Proceedings of Eighth Rock Mechanics Symposium*, pp. 45–52, American Rock Mechanics Association, Minneapolis, MN, USA, September 1966.

[11] H. S. Mitri, B. Tang, and R. Simon, "FE modelling of mining-induced energy release and storage rates," *Journal of the South African Institute of Mining and Metallurgy*, vol. 99, pp. 103–110, 1999.

[12] T. D. Wiles, "Correlation between local energy release density observed bursting conditions at Creighton mine," *Sudbury*, vol. 20, pp. 101–115, 1998.

[13] Q. Jiang, X. T. Feng, T. B. Xiang, and G. S. Su, "Rockburst characteristics and numerical simulation based on a new energy index: a case study of a tunnel at 2,500 m depth," *Bulletin of Engineering Geology and the Environment*, vol. 69, no. 3, pp. 381–388, 2010.

[14] J. Xu, J. Jiang, N. Xu, Q. Liu, and Y. Gao, "A new energy index for evaluating the tendency of rockburst and its engineering application," *Engineering Geology*, vol. 230, pp. 46–54, 2017.

[15] N. I. Aziz and W. Ming-Li, "The effect of sorbed gas on the strength of coal–an experimental study," *Geotechnical and Geological Engineering*, vol. 17, no. 3/4, pp. 387–402, 1999.

[16] B. B. Beamish and P. J. Crosdale, "Instantaneous outbursts in underground coal mines: an overview and association with coal type," *International Journal of Coal Geology*, vol. 35, no. 1–4, pp. 27–55, 1998.

[17] B. Hodot, *Coal and Gas Outbursts*, Coal Industry Press, Beijing, China, 1966.

[18] W. Zhao, Y. Cheng, H. Jiang, K. Jin, H. Wang, and L. Wang, "Role of the rapid gas desorption of coal powders in the development stage of outbursts," *Journal of Natural Gas Science and Engineering*, vol. 28, pp. 491–501, 2016.

[19] P. Guan, H. Wang, and Y. Zhang, "Mechanism of instantaneous coal outbursts," *Geology*, vol. 37, no. 10, pp. 915–918, 2009.

[20] С. Г. Авершин, *Rockburst*, China Coal Industry Publishing House, Beijing, China, 1959.

[21] G. Bräuner, *Mine Pressure and Rockburst*, China Coal Industry Publishing House, Beijing, China, 1985.

[22] T. Li, M. F. Cai, J. A. Wang et al., "Discussion on relativity between rockburst and gas in deep exploitation," *Journal of China Coal Society*, vol. 30, pp. 562–567, 2005.

[23] F. M. Zhang, Z. Y. Yu, X. Y. Xu et al., "Research on induced earthquakes by coal mining in Hegang," *Journal of Natural Disasters*, vol. 14, pp. 139–143, 2005.

[24] F. W. Zhang and T. Li, "Cognizance on compound dynamic disaster of coal and gas in deep mining," *Zhongzhou Coal*, vol. 106, pp. 73–76, 2009.

[25] Y. C. Lu, "Technology of bumping prevention and control for gateway driving in seam with outburst in potential," *Coal Science and Technology*, vol. 36, pp. 43–46, 2008.

[26] Petukhov, *Coal Mine Rock Burst*, China Coal Industry Publishing House, Beijing, China, 1992.

[27] А. Т. Айруни, *Prediction and Prevention of Gas Dynamic Phenomena in Mines*, China Coal Industry Publishing House, Beijing, China, 1992.

[28] K. Ogieglo, M. Lubryka, J. Kutkowski et al., "Influence of mine shock to gas emission rate," *Ground Pressure and Strata Control*, vol. 22, pp. 109–111, 2005.

[29] M. T. Zhang, Z. H. Xu, Y. S. Pan et al., "A united instability theory on coal (rock) burst and outburst," *Journal of China Coal Society*, vol. 16, pp. 48–53, 1991.

[30] Y. S. Pan, Z. H. Li, and M. T. Zhang, "Distribution type mechanism and prevention of rockburst in China," *Chinese Journal of Rock Mechanics and Engineering*, vol. 22, pp. 1844–1851, 2003.

[31] S. Y. Li, X. S. He, K. Pan et al., "Relationship between mining seismicity and gas outburst in coal mine," *Journal of China Coal Society*, vol. 31, pp. 11–18, 2006.

[32] T. Li, T. T. Mei, G. Q. Li et al., "Mechanism study of coal and gas outburst induced by rockburst in "three-soft" coal seam," *Chinese Journal of Rock Mechanics and Engineering*, vol. 30, pp. 1283–1288, 2011.

[33] Z. Wang, G. Z. Yin, Q. T. Hu et al., "Inducing and transforming conditions from rockburst to coal-gas outburst in a high gassy coal seam," *Journal of Mining & Safety Engineering*, vol. 27, pp. 572–575, 2010.

[34] B. Wu, W. Yao, and K. Xia, "An experimental study of dynamic tensile failure of rocks subjected to hydrostatic confinement," *Rock Mechanics and Rock Engineering*, vol. 49, no. 10, pp. 3855–3864, 2016.

[35] Y. Xue, P. G. Ranjith, F. Gao et al., "Mechanical behaviour and permeability evolution of gas-containing coal from unloading confining pressure tests," *Journal of Natural Gas Science and Engineering*, vol. 40, pp. 336–346, 2017.
[36] Y. Xue, F. Gao, and X. Liu, "Effect of damage evolution of coal on permeability variation and analysis of gas outburst hazard with coal mining," *Natural Hazards*, vol. 79, no. 2, pp. 999–1013, 2015.
[37] Y. Al-Salloum, T. Almusallam, S. M. Ibrahim, H. Abbas, and S. Alsayed, "Rate dependent behavior and modeling of concrete based on SHPB experiments," *Cement and Concrete Composites*, vol. 55, pp. 34–44, 2015.
[38] S. S. Daryadel, P. R. Mantena, K. Kim, D. Stoddard, and A. M. Rajendran, "Dynamic response of glass under low-velocity impact and high strain-rate SHPB compression loading," *Journal of Non-crystalline Solids*, vol. 432, pp. 432–439, 2016.
[39] S. Mishra, T. Chakraborty, and V. Matsagar, "Dynamic characterization of Himalayan quartzite using SHPB," *Procedia Engineering*, vol. 191, pp. 2–9, 2017.
[40] E. Kim and H. Changani, "Effect of water saturation and loading rate on the mechanical properties of red and buff sandstones," *International Journal of Rock Mechanics and Mining Sciences*, vol. 88, pp. 23–28, 2016.
[41] R. L. Shan, R. Q. Cheng, and W. J. Gao, "Study on dynamic constitutive model of anthracite of Yunjialing coal mine," *Chinese Journal of Rock Mechanics and Engineering*, vol. 25, pp. 2258–2263, 2006.
[42] X. H. Liu, R. Zhang, and J. F. Liu, "Dynamic test study of coal rock under different strain rates," *Journal of China Coal Society*, vol. 37, pp. 1528–1534, 2012.
[43] C. M. Mu and N. P. Gong, "Damage mechanism of coal under impact loads," *Journal of China Coal Society*, vol. 42, pp. 2011–2018, 2017.
[44] L. F. Rong, C. M. Mu, and W. Q. Zhang, "Mechanical properties and establishment of constitutive relation of coal rock in 13-1 coal seam from Panxie coalfield under impact load," *Journal of China Coal Society*, vol. 40, pp. 40–46, 2015.
[45] X. G. Kong, S. G. Li, E. Y. Wang et al., "Dynamics behaviour of gas-bearing coal subjected to SHPB tests," *Composite Structures*, vol. 256, Article ID 113088, 2021.
[46] X. G. Kong, E. Y. Wang, S. G. Li, H. Lin, Z. Zhang, and Y. Ju, "Dynamic mechanical characteristics and fracture mechanism of gas-bearing coal based on SHPB experiments," *Theoretical and Applied Fracture Mechanics*, vol. 105, Article ID 102395, 2020.
[47] M. C. He, G. X. Yang, J. L. Miao et al., "Classification and research methods of rockburst experimental fragments," *Chinese Journal of Rock Mechanics and Engineering*, vol. 28, pp. 1521–1529, 2009.
[48] Q. T. Hu, *Study on the Mechanical Mechanism of Coal and Gas Outburst and Its Application*, China University of Mining and Technology, Beijing, China, 2007.
[49] В. В. Ходот, *Coal and Gas Outburst*, China Industry Press, Beijing, China, 1966.
[50] X. C. Zhang and X. X. Miao, "Numerical simulation of layer-c rack and failure of laminated rock masses," *Chinese Journal of Rock Mechanics and Engineering*, vol. 21, pp. 1645–1650, 2002.